RSC Advances

PAPER

View Article Online
View Journal | View Issue

Cite this: *RSC Adv.*, 2022, **12**, 34797

Colour-tuneable solid-state fluorescence of crystalline powders formed from push–pull substituted 2,5-diphenyl-stilbenes†

Karel Pauk,[a] Stanislav Luňák, Jr,[b] Aleš Růžička,[c] Aneta Marková,[b] Kateřina Teichmanová,[a] Anna Mausová,[a] Matouš Kratochvíl,[b] Rastislav Smolka,[b] Tomáš Mikysek,[d] Martin Weiter,[b] Aleš Imramovský*[a] and Martin Vala*[b]

The solid-state fluorescence (SSF) of eight DPA–DPS-EWG derivatives (DPA = diphenylamino, DPS = 2,5-diphenyl-stilbene building block, EWG = electron withdrawing group) was studied. Varying the strength of the EWG enabled the tuning of the LUMO energy within a range broader than 1 eV, while the simultaneous changes of HOMO energy were less than 0.1 eV, according to cyclic voltammetry. The fluorescence maxima in dichloromethane laid between 483 and 752 nm and exhibited monoexponential decay and a photoluminescence quantum yield (PLQY) always higher than 35%. Six derivatives with a SSF PLQY higher than 10% in polycrystalline powder form continuously covered the range from 475 to 733 nm. Three components of SSF multiexponential decay, obtained by time-resolved fluorescence spectroscopy, were ascribed to exciton migration to nonfluorescent traps, and monomer-like and aggregate fluorescence. The character of the emitting aggregates was evaluated by quantum chemical modelling based on time-dependent density functional theory computations, carried out on the dimer arrangements obtained by X-ray diffractometry of the single crystals.

Received 5th September 2022
Accepted 18th November 2022

DOI: 10.1039/d2ra05593g

rsc.li/rsc-advances

Introduction

Luminescent materials based on all-organic conjugated molecules are usually used in solid physical form in technological fields, such as biological probes, chemical sensing, optoelectronic systems and stimuli-responsive materials.[1] Solid-state fluorescence (SSF) has been studied on single crystals, polycrystalline powders, thin films and nanostructures.[2] Typical applications of single-crystal emission are in lasing and organic light-emitting field-effect transistors,[3–6] fluorescent powders are common in stimuli-responsive research,[7,8] thin films/layers form a key component of organic light-emitting diodes[9–13] and water dispersions of nanoparticles dominate biomedical studies.[14–19] The efficiency of SSF depends on the combination of nonradiative intramolecular deactivation processes, intermolecular arrangement and morphology, the net effect of which can cause either quenching or enhancement of the photoluminescence quantum yield (PLQY) compared to solution.[20] Intramolecular nonradiative pathways occur either with a conserved spin (internal conversion, IC) or with a spin-flip (intersystem crossing, ISC), both of which are often supported by large-amplitude excited-state structural motions.[20,21] Solidification is, thus, a way to improve PLQY by limiting these vibrations/rotations *via* various mechanisms.[20,22] The mutual arrangement of the molecules in crystals determines their photophysics through excitonic coupling, forming physical J- or H-aggregates unambiguously defined by the bright (oscillator strength $f_{osc} > 0$) or dark ($f_{osc} \sim 0$) character of the lowest excited state, respectively.[23,24] True H-aggregates, determined by a decrease in the radiative rate of a solid with respect to a solution, *i.e.* not only by geometrical factors, are more common than J-aggregates, and it is believed that their SSF is enabled by static and/or dynamic symmetry breaking enhancing the f_{osc} of the H-aggregate lowest state.[20] Excitons formed during photon absorption are either localised by self-trapping or delocalised over several molecules, and they may migrate in crystals and fall into various traps, either in bulk or on the surface.[25] This trapping is generally considered to be the main source of SSF quenching in solids, and a higher concentration of traps on the surface and a shorter distance from the excited site to the surface lead to a common decrease in the PLQY when transitioning from single crystals to polycrystalline

[a]*Institute of Organic Chemistry and Technology, Faculty of Chemical Technology, University of Pardubice, Studentská 95, Pardubice CZ-530 09, Czech Republic. E-mail: ales.imramovsky@upce.cz*

[b]*Materials Research Centre, Faculty of Chemistry, Brno University of Technology, Purkyňova 464/118, Brno CZ-612 00, Czech Republic. E-mail: vala@fch.vut.cz*

[c]*Department of General and Inorganic Chemistry, Faculty of Chemical Technology, University of Pardubice, Studentská 573, Pardubice CZ-532 10, Czech Republic*

[d]*Department of Analytical Chemistry, Faculty of Chemical Technology, University of Pardubice, Studentská 573, Pardubice CZ-532 10, Czech Republic*

† Electronic supplementary information (ESI) available. CCDC 2118685 and 2118686. For ESI and crystallographic data in CIF or other electronic format see DOI: https://doi.org/10.1039/d2ra05593g

powders, films and nanoparticles.[20] Consequently, reducing exciton migration is one of the few general ways to obtain highly luminescent poly- and nanocrystalline organic solids.[20]

Exciton traps are often connected with cofacial H-aggregates.[26] If they both fulfil the conditions of limited delocalisation on only two molecules and show a pronounced charge-transfer (CT) character, they can be called excimers.[27] On the other hand, an excimer-induced enhanced emission[28] phenomenon has been observed on crystals, formed by discrete pairwise π–π stacked dimers of polycyclic aromatic hydrocarbons, such as perylene[28] or anthracene,[29,30] suitably substituted by bulk groups. Excimer-type SSF can also originate from crystals with alternating (*e.g.* stacked/unstacked) dimers in columns;[31] however, relatively small changes in the molecular structure, saving the same building block, may transform this unique arrangement into uniform columns with either H- or J-type aggregation.[32,33] We have recently observed that one of the polymorphs of **DPA-DPS-DCV** (Chart 1) forms a crystal arrangement with such alternating dimers and consequent intense infrared excimer-type emission was observed.[34] Research on solid-state emitters has paid special attention to the series of derivatives based on the same building block with SSF maxima tuned by a variation of simple substituents.[35–37] An impressive interval of SSF maxima from 383 to 631 nm, *i.e.* covering a range of 248 nm (1.27 eV), obtained by varying the electron withdrawing group (EWG) on simple triphenylamines,[38] shows the potential of this approach, *e.g.* for multicomponent white-light-emitting materials.[39]

Recently, we synthesised[34] **DPA-DPS-CHO** (Chart 1), a synthetic precursor of **DPA-DPS-DCV**, with a push–pull substituted stilbene π-system decorated at the acceptor part by a pair of side-phenyls. Both polymorphs of **DPA-DPS-CHO** have shown green monomer-type SSF with only moderate PLQY. Side-phenyl interactions (CH–π or π-stacking) in **DPA-DPS-CHO** and **DPA-DPS-DCV**, respectively, were found to be vital for an overall crystalline arrangement of molecules and the consequent SSF ability. Here we present further research into additional DPA-DPS-EWG derivatives, synthesised from **DPA-DPS-CHO**, in order to cover a much broader area of SSF colours by tuning the EWG strength within a series of emitters based on the same donor (DPA) and the same building block (DPS). Attention was paid to the relationship between the acceptor strength and SSF spectra (energy), and between the crystal structure and photophysics (PLQY and fluorescence decay), in order to better understand the nature of the SSF phenomenon in polycrystalline solids. The series was designed to answer, at minimum, the following questions. (1) Is the presence of side-phenyl substituents a universal way of achieve SSF of at least moderate intensity? (2) Does the intensity of SSF follow the so-called "energy gap law", usually indicating intramolecular internal conversion as a dominant deactivation pathway, as sometimes found in isolated molecules?[20] (3) Is the crystal arrangement consisting of alternating stacked/unstacked dimers, as observed for **DPA-DPS-DCV**,[34] driven by side-phenyl specific interactions which lead to excimer-induced fluorescence unique or quite common in a series of isostructural compounds differing only by EWG substituent?

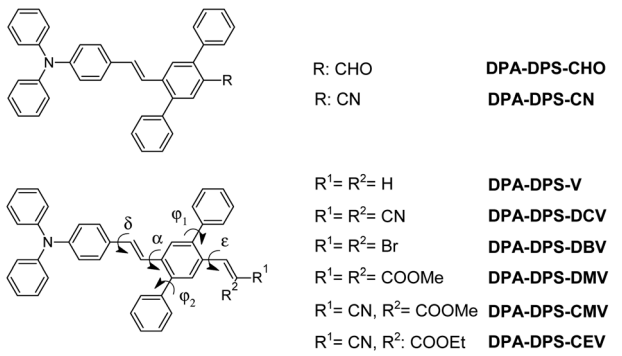

Chart 1 Notations of the compounds under study.

Experimental

Synthesis

All reagents and solvents were purchased from commercial sources (Sigma-Aldrich, Fluorochem, Acros Organics, TCI Europe, Merck, and Lach-Ner). Commercial grade reagents were used without further purification. Reactions were monitored using thin layer chromatography (TLC) plates coated with 0.2–0.5 mm silica gel (60 F254, Merck). TLC plates were visualised using UV irradiation (254 nm). All melting points were determined using a melting point B-540 apparatus (Büchi, Switzerland) and are given in their uncorrected form. Fourier transform infrared (FT-IR) spectra were recorded on a Nicolet iS50 using the ATR technique. The NMR spectra were measured in $CDCl_3$ and CD_2Cl_2-d_2 solvents at ambient temperature using either a Bruker Avance™ III 400 spectrometer at frequencies of 400 MHz (^{1}H) and 100.26 MHz (^{13}C), or a Bruker Ascend™ 500 spectrometer at frequencies of 500.13 MHz (^{1}H) and 125.76 MHz ($^{13}C\{^1H\}$). The chemical shifts (δ) reported in the ESI† are given in ppm and are related to the following residual solvent peaks: −4.79 (D_2O-d_2), −5.32 (CD_2Cl_2-d_2) and −7.27 ($CDCl_3$). Tetramethylsilane (TMS) was used as an internal standard. The coupling constants (J) are reported in Hz. Elemental analyses (C, H, and N) were performed on an automatic microanalyser (Flash 2000 Organic elemental analyser). High-resolution mass spectrometry was performed by the "dried droplet" method using the MALDI mass spectrometer LTQ Orbitrap XL (Thermo Fisher Scientific) equipped with a nitrogen UV laser (337 nm, 60 Hz). Spectra were measured in positive ion mode and in regular mass extent with a resolution of 100 000 at a mass-to-charge ratio (m/z) of 400, with 2,5-dihydrobenzoic acid (DBH) used as the matrix.

Single-crystal X-ray diffraction (XRD)

Full-sets of diffraction data for **DPA-DPS-CMV** and **DPA-DPS-DMV** were collected at 150(2) K with a Bruker D8-Venture diffractometer equipped with Cu (Cu/K_α radiation; λ = 1.54178 Å) or Mo (Mo/K_α radiation; λ = 0.71073 Å) microfocus X-ray (IμS) sources, a Photon CMOS detector and an Oxford Cryosystems cooling device. The frames were integrated with the

Bruker SAINT software package using a narrow-frame algorithm. Data were corrected for absorption effects using the Multi-Scan method (SADABS). The obtained data were treated by XT-version 2017/1 and SHELXL-2014/7 software implemented in the APEX3 v2017.1-0 (Bruker AXS) system. CCDC 2118685 and 2118686 contains the ESI† crystallographic data for this paper.

Electrochemical measurements

Electrochemical measurements were carried out in acetonitrile containing 0.1 M Bu_4NPF_6 in a three-electrode cell by cyclic voltammetry (CV) and rotating disk voltammetry (RDV). For CV and RDV experiments, the working electrode was a glassy carbon disk (3 mm in diameter). A saturated calomel electrode (SCE) separated by a bridge filled with supporting electrolyte and Pt wire were used as the reference and auxiliary electrodes. All potentials are given *vs.* SCE. Voltametric measurements were performed using a potentiostat PGSTAT 128N (AUTOLAB, Metrohm Autolab B.V., Utrecht, The Netherlands) operated *via* NOVA 1.11 software.

Spectral and photophysical measurements

UV-vis absorption was measured by employing a Varian Cary Probe 50 UV-Vis spectrometer (Agilent Technologies Inc.). Steady-state photoluminescence was captured using an SF5 spectrofluorometer (Edinburgh Instruments). Photoluminescence quantum yields (PLQYs) were determined by the absolute method employing an integrating sphere SC-30 (Edinburgh Instruments). PLQYs of powdered samples were determined by a combination of direct and indirect excitation. Time-resolved fluorescence was recorded by means of the time-correlated single photon counting method (TCSPC) using a Horiba Jobin Yvon Fluorocube.

Quantum chemical calculations

Monomer geometries in the ground and the lowest excited state were optimised by density functional theory (DFT) and time-dependent (TD) DFT calculations, respectively. Either ωB97X-D[51] or CAM-B3LYP[52] xc functionals, and either 6-31G(d,p) or 6-311G(d,p) basis sets were used. The solvent effect was introduced by the polarised continuum model (PCM). Excitation energies of the dimers (and monomers, for comparison) were calculated by the TD DFT ωB97X-D/6-311G(d,p) level in vacuum on the geometries obtained from single-crystal XRD. All calculations were carried out with Gaussian 09 software.[40]

Results and discussion

The synthesis of new compounds was carried out according to Scheme 1. In most cases, the previously reported[34] **DPA-DPS-CHO** was used as the starting precursor. The only exception were the syntheses of **DPA-DPS-CN**, for which an independent synthesis according to Scheme 1 gave a considerably better yield and purity compared to the oxidation of **DPA-DPS-CHO** with iodine in NH_4OH, which provided an inseparable mixture of substances. Final powders for SSF measurements were obtained by crystallisation from ethyl acetate (**DPA-DPS-CN**, **-V** and **-DBV**), DCM (**DPA-DPS-CMV**) or an EtOAc/MeOH/*n*-hexane/DCM

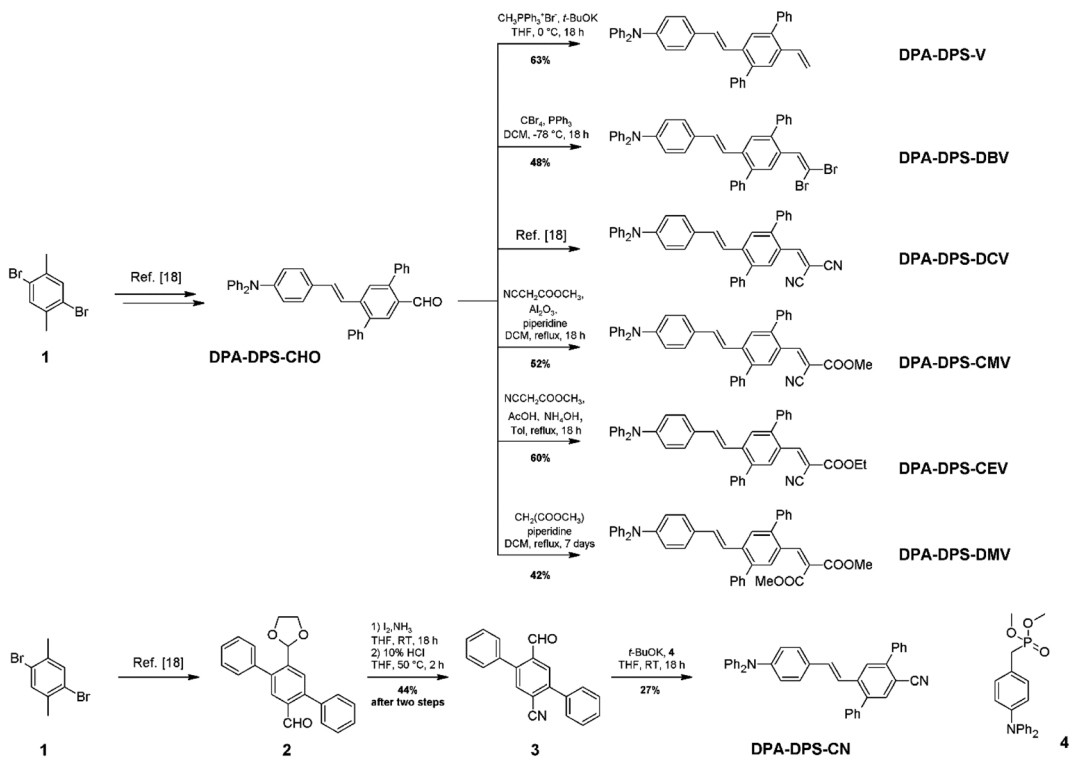

Scheme 1 Synthesis of DPA-DPS-EWGs. Compound 4 = dimethyl (4-(diphenylamino)benzyl)phosphonate.

mixture (**DPA-DPS-DMV** and **-CEV**), only dried, without any physical treatment.

Single crystals of **DPA-DPS-DMV** and **DPA-DPS-CMV**, obtained by crystallisation from solution, were prepared in a quality suitable for X-ray diffraction (XRD) analysis. The former crystallises in a non-centrosymmetrical $P2_12_12_1$ space group (such as **DPA-DPS-CHO**),[34] and the latter in a centrosymmetrical $P2_1/c$ group (**DPA-DPS-DCV** crystallizes in a different centrosymmetrical $P1$ space group).[34] A unit cell of all four derivatives consists of four molecules ($Z = 4$) and contains only one independent molecule. The molecular geometries of both **DPA-DPS-DMV** and **DPA-DPS-CMV** in crystals are mutually similar (Fig. 1). Contrary to **-CHO** and **-DCV** derivatives, which have nearly coplanar side-phenyls, *i.e.* out-of-plane rotated in the same manner (*e.g.* $\varphi_1 = -53.5°$ and $\varphi_2 = +46.0°$ for **-DCV**), the phenyls in **-DMV** and **-CMV** derivatives are rotated out-of-plane in a mutually opposite manner ($\varphi_1 = +61.2°$ and $\varphi_2 = +46.2°$ for CMV and $\varphi_1 = -65.0°$ and $\varphi_2 = -52.5°$ for DMV). As for **-CHO** and **-DCV** compounds,[34] the stilbene units in both derivatives are non-planar ($\alpha = +29.9°$, $\delta = -1.6°$ and $\varepsilon = -24.4°$ for **-CMV**, and $\alpha = -29.2°$, $\delta = -10.5°$ and $\varepsilon = +6.0°$ for **-DMV**), *i.e.* considerably more distorted than in analogous compounds without side-phenyls.[41,42]

Molecules of **DPA-DPS-DMV** form infinite stacked columns consisting of the same type of non-centrosymmetrical dimer with parallel dipole moments (Fig. 2). The key intermolecular interactions that form the columns are of the edge-to-face C–H···π type. Contrary to **DPA-DPS-CHO**, where y-shaped C–H···π interactions connected the side-phenyls of adjacent molecules,[34] in DPA-DPS-DMV, these interactions are of a T-shape[43] and form a network with multiple contacts either between the side-phenyls and the phenyls of a DPA group, or between the phenyls of triphenylamine groups mutually.

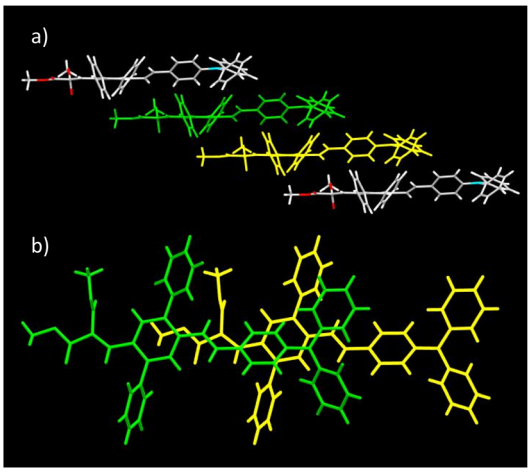

Fig. 2 Crystal structure of DPA-DPS-DMV. Overall view (a) of the stacked column. Detailed view of a stacked dimer with PP = 3.445 Å (b).

As for **DPA-DPS-DCV**,[34] the molecules of **DPA-DPS-CMV** form slipped infinite columns with two alternating (stacked/unstacked) types of centrosymmetrical dimer with antiparallel dipole moments (Fig. 3). In contrast to **DPA-DPS-DCV**, the stacked dimer 1 is shorter (NN = 16.636 Å) than the unstacked

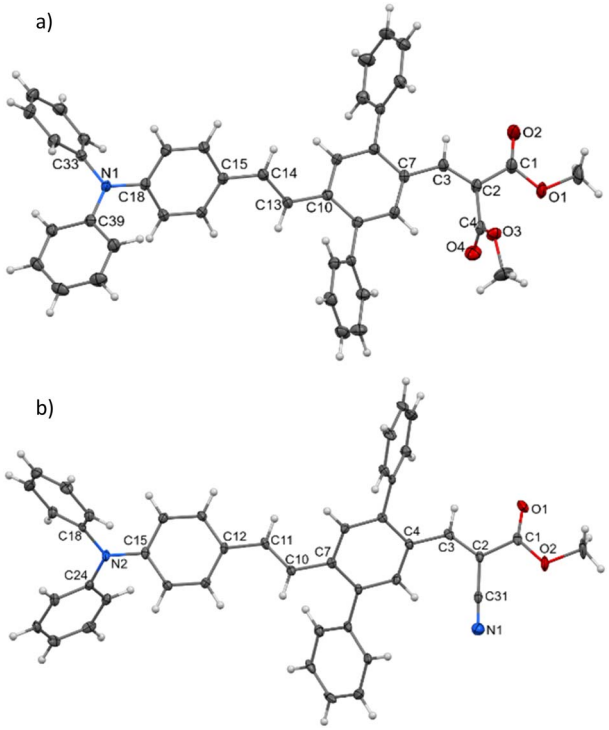

Fig. 1 Molecular structure of DPA-DPS-DMV (a) and DPA-DPS-CMV (b), ORTEP view, 50% probability level.

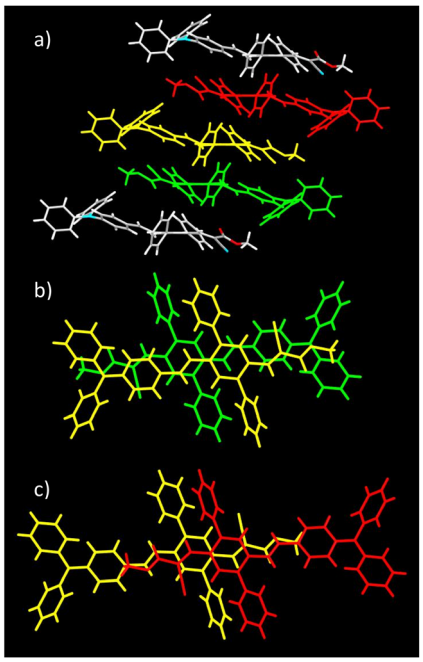

Fig. 3 Crystal structure of DPA-DPS-CMV. Overall view (a) of the alternation of the dimers in a slipped stacked column. Dimer 1 consists of yellow and green monomers, and dimer 2 of yellow and red monomers. Detailed view of stacked dimer 1 (b) with PP = 3.449 Å. Detailed view of unstacked dimer 2 (c) with PP = 4.291 Å.

dimer 2 (NN = 21.221 Å). The dimer forming an interaction between adjacent molecules in **DPA-DPS-CMV** columns is created by T-shape C–H···π type connections exclusively between side-phenyls. Such a decisive role of side-phenyls was also observed in **DPA-DPS-DCV**, in which case the side-phenyls were coupled by parallel offset face-to-face stacks.[34]

The geometry of both alternating dimers 1 and 2 of **DPA-DPS-CMV** (Fig. 3) was recomputed from crystal structures by DFT (ωB97X-D/6-31G(d,p))[40] and compared with the experimental data. The computed structure of dimer 1 matches the experiment quite well and dimer 1 can, thus, be considered as a standalone dimer. The overall length of a conjugated system of this dimer, characterised by a distance between the nitrogens of TPA groups (NN), was found to be 16.501 Å (exp. NN = 16.636 Å). The plane-to-plane (PP) distance, defined by the central benzene rings of the 2,5-diphenyl-1,4-divinyl-benzene (PVB) unit, was computed to be 3.286 Å (exp. PP = 3.448 Å), signalising a slightly overestimated dispersion attractive force with respect to repulsive electron exchange in the ωB97X-D xc functional, as in the previously studied case of **DPA-DPS-DCV**.[33] However, the experimental arrangement of the unstacked dimer 2 could not be well reproduced, because (1) the optimised geometry always converged to a dimer with coplanar stacked side-phenyls, and (2) the NN distances were always significantly shorter (by more than 0.5 Å) than the experimental ones. The computations of the stacked dimer of **DPA-DPS-DMV** (Fig. 2) failed entirely as it was impossible to reproduce the coplanarity of the central benzene rings of adjacent molecules. Consequently, all reported energies of the dimers (*vide infra*) were obtained by (time-dependent) density functional theory [(TD) DFT] calculations, carried out on non-optimised geometries obtained from XRD single-crystal structures.

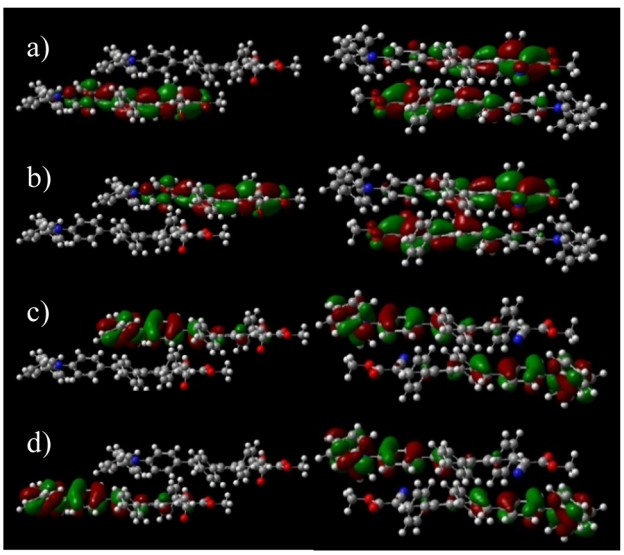

Fig. 4 Split orbitals LUMO+1 (a), LUMO (b), HOMO (c) and HOMO−1 (d) in a dimer of DPA-DPS-DMV (left) and dimer 1 of DPA-DPS-CMV (right). DFT calculations were carried out on the wB97X-D/6-31G(d,p) level. An isovalue of 0.02 was used for the drawing.

Although **DPA-DPS-CMV** forms columns of stacked/unstacked alternating centrosymmetrical dimers such as **DPA-DPS-DCV**, the more compact arrangement of a stacked dimer 1 for the former derivative significantly affects the electronic properties expressed in terms of split frontier Kohn–Sham orbitals (KS FMOs). First, the symmetries of the HOMO (a_u) and HOMO−1 (a_g) are the same for both derivatives, but the symmetries of the LUMO (a_g) and LUMO+1 (a_u) of **DPA-DPS-CMV** (Fig. 4) are opposite to the FMOs of **DPA-DPS-DCV**, *i.e.* during the slipping, longitudinal geometrical shift virtual orbitals pass a node.[44]

Second, the virtual orbital energy splitting (ΔLUMO = 108 meV), relating to electron transfer, is lower, while the occupied orbital splitting (ΔHOMO = 73 meV), relating to hole transfer, is higher than for **DPA-DPS-DCV**, *i.e.* both transfer integrals are better balanced for **DPA-DPS-CMV**. Third, FMOs in an antiparallel arrangement of **DPA-DPS-CMV** are delocalised over both molecules in a dimer with a significant overlap in the LUMO, contrary to parallelly packed **DPA-DPS-DMV** (Fig. 4), in which all four KS orbitals are localised on only one molecule, with a consequent low orbital energy splitting (ΔHOMO = 24 meV and ΔLUMO = 19 meV).

The strength of acceptor substituents in push–pull substituted derivatives was related to the LUMO energy obtained from cyclic voltammetry (Table 1). The representative CV curves of the compounds with the highest (**DPA-DPS-V**) and the lowest (**DPA-DPS-DCV**) LUMO are shown in Fig. 5 together with a visualised HOMO and LUMO dependence on the EWG. CV curves for further compounds can be found in the ESI.† HOMO

Table 1 Results of cyclic voltammetry. $E_{(ox1)}$ ($E_{(red1)}$) stands for the potentials of the first oxidation (reduction)[a]

Material	$E_{(ox2)}$ [V]	$E_{(ox1)}$ [V]	$E_{(red1)}$ [V]	HOMO [eV]	LUMO [eV]	ΔHL [eV]
DPA-DPS-V	0.929	0.794	−2.032	−5.223	−2.397	2.83
DPA-DPS-DBV	0.947	0.807	−1.682	−5.236	−2.747	2.49
DPA-DPS-CN	0.944	0.855	−1.741	−5.284	−2.688	2.60
DPA-DPS-CHO	0.977	0.854	−1.564	−5.283	−2.866	2.42
DPA-DPS-DMV	0.982	0.813	−1.444	−5.242	−2.985	2.26
DPA-DPS-CEV	0.994	0.838	−1.133	−5.267	−3.296	1.97
DPA-DPS-CMV	0.984	0.819	−1.126	−5.248	−3.303	1.95
DPA-DPS-DCV	1.005	0.862	−0.949	−5.291	−3.480	1.81

[a] HOMO/LUMO energies were computed from oxidation/reduction potentials according to the formula $-E_{HOMO/LUMO}$ [eV] = $E_{(ox1/red1)}$ [V] + 4.429 (ref. 45).

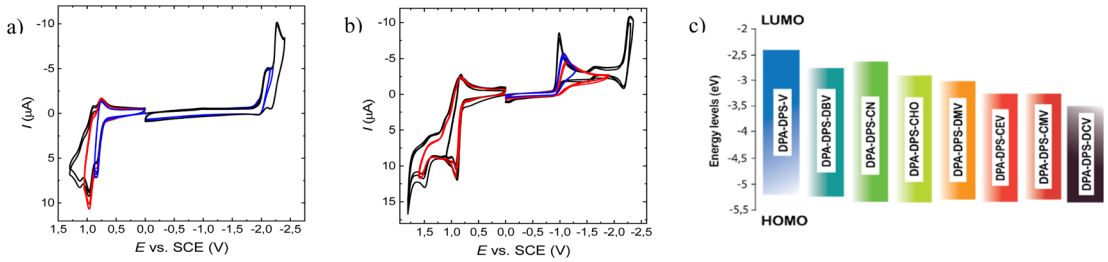

Fig. 5 Representative CV curves of the oxidation and reduction of **DPA-DPS-V** (a) and **DPA-DPS-DCV** (b) compounds at the glassy carbon electrode in acetonitrile containing 0.1 M Bu_4NPF_6.; $v = 100$ mV s^{-1}. Visualisation of HOMO and LUMO levels (c) from Table 1.

energies in the set under study are only slightly affected by the EWG, within 0.07 eV, while the effect on the LUMO is dramatic. The double cyanation of **DPA-DPS-V** to **DPA-DPS-DCV** decreases its energy by more than 1.08 eV. The difference between the electrochemical gaps of these compounds is (consequently) also higher than 1 eV, *i.e.* the set based on the same donor (DPA) and building block (DPS) is suitable for wide-range tuning of the spectral properties.

Absorption and fluorescence spectra in solution show dependencies that are clear and expected for push–pull compounds (Tables S3–S9†). They show a bathochromic shift (Fig. 6a) and a more pronounced bathofluoric (Fig. 6b) shift with an increasing electron-acceptor strength of the EWG. The effect of side-phenyls on the spectra of **DPA-DPS-CN** (with respect to DPA-stilbene-CN) is qualitatively similar to the reported shifts for an analogous substituted pair with EWG = CHO,[34] *i.e.* **DPA-DPS-CN** shows a small red shift in absorption (5 nm) and a moderate shift in fluorescence (33 nm), both in acetonitrile.[46] Positive fluorescence solvatochromism is more distinct for the compounds with a strong EWG; the effect is given both by a stronger solute–solvent interaction and the redistribution of a vibronic pattern from a 0–0 (typically **DPA-DPS-V** in less polar solvents, Fig. 6c) to a 0–1 (typically **DPA-DPS-CMV** in more polar solvents, Fig. 6d) maximum. This effect relates to the solvent-dependent structural relaxation in the S_1 (HOMO–LUMO) state (Table 2). DFT calculated exocyclic bond lengths in S_0 are independent of solvent within 0.001 Å and show a remarkable agreement with experimental values (computed C=C bond lengths in toluene are only 0.003 Å longer than those obtained from single-crystal XRD). Irrespective of the solvent, TD DFT calculated excitation to S_1 is accompanied by the planarization of a main conjugated chain on account of a more pronounced side-phenyl torsion. However, the bond length alternation (BLA) of exocyclic bonds is considerably dependent on the solvent, *e.g.* the terminal C=C bond (bond e in Table 2) of **DPA-DPS-DCV** is lengthened by 0.011 Å when changing the solvent from toluene to acetonitrile. This change in BLA causes a solvent-dependent shift of the S_1 hypersurface with respect to S_0 along the C=C coordinate, responsible for the main vibronic progressions in conjugated compounds,[47] and consequent modifications of Franck–Condon factors, responsible for vibronic band intensities. Such a redistribution of vibronic intensities affects, of course, the

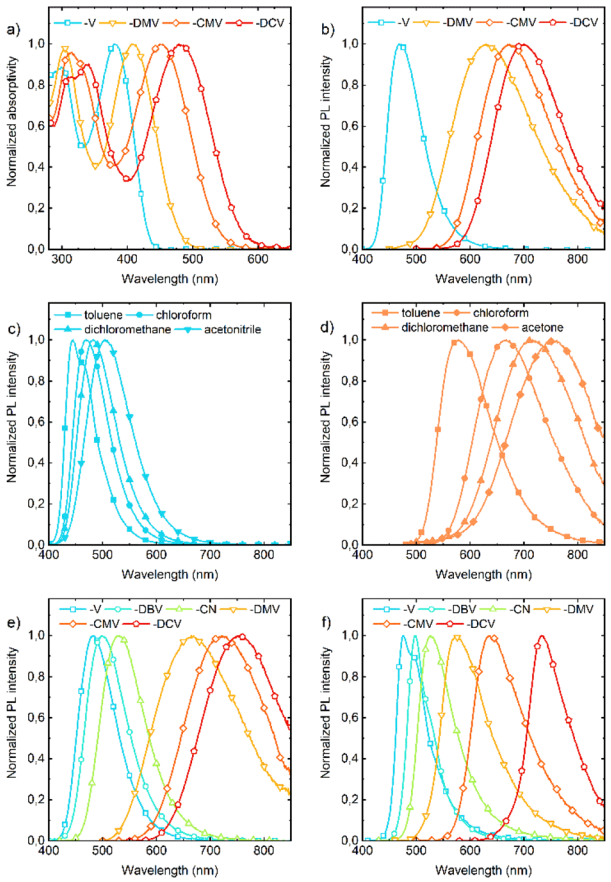

Fig. 6 Absorption (a) and fluorescence (b) spectra of **DPA-DPS-V**, **-DMV**, **-CMV** and **-DCV** in chloroform. Fluorescence of **DPA-DPS-V** (c) and **-CEV** (d) in toluene, chloroform, dichloromethane and acetonitrile (**-V**) or acetone (**-CEV**). Fluorescence of **DPA-DPS-V**, **-DBV**, **-CN**, **-DMV**, **-CMV** and **-DCV** in dichloromethane (e) and the solid-state (f).

Stokes shift in solvents of moderate polarity (Table 3). Its highest value in all solvents was found for **DPA-DPS-DMV**, both experimentally and theoretically, due to the more energetic geometrical relaxation of the ester with respect to the cyano group. While the differences between the computed and measured values are relatively consistent for the three compounds with the strongest EWG, this difference found for **DPA-DPS-V** is about 2000 cm^{-1} higher in all solvents. This discrepancy arises from the vibronic structure, *i.e.* the Stokes

Table 2 Experimental (XRD) and PCM (TD) DFT (ωB97X-D/6-31G(d,p)) optimised exocyclic C=C/C–C bond lengths of a monomer in S_0 and S_1 states (SS = solid-state, all values in Å)

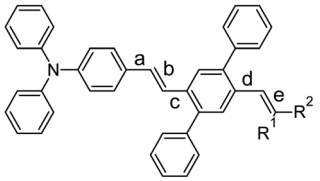

			Bond length [Å]				
$R_1 = R_2$	State	Solvent	a	b	c	d	e
H	S_0	SS (exp.)	—	—	—	—	—
		CH_3Ph	1.469	1.340	1.472	1.477	1.334
	S_1	CH_3Ph	1.404	1.407	1.407	1.459	1.342
		$CHCl_3$	1.402	1.410	1.405	1.459	1.343
		CH_2Cl_2	1.400	1.412	1.403	1.458	1.343
		CH_3CN	1.399	1.414	1.402	1.458	1.344
COOMe	S_0	SS (exp.)	1.458	1.338	1.465	1.463	1.342
		CH_3Ph	1.467	1.341	1.470	1.466	1.344
	S_1	CH_3Ph	1.409	1.401	1.405	1.429	1.369
		$CHCl_3$	1.406	1.404	1.402	1.426	1.372
		CH_2Cl_2	1.404	1.406	1.400	1.423	1.374
		CH_3CN	1.402	1.408	1.397	1.421	1.376
CN	S_0	SS (exp.)	1.462	1.338	1.465	1.454	1.351
		CH_3Ph	1.467	1.341	1.469	1.457	1.357
	S_1	CH_3Ph	1.412	1.396	1.408	1.417	1.393
		$CHCl_3$	1.408	1.400	1.404	1.412	1.398
		CH_2Cl_2	1.405	1.403	1.401	1.409	1.401
		CH_3CN	1.402	1.406	1.398	1.405	1.404

shift for all three **DPA-DPS-DMV**, **-CMV** and **-DCV** compounds is estimated between 0–1 maxima both in absorption and fluorescence, while for **DPA-DPS-V**, the Stokes shift is the difference between the 0–1 absorption maximum and the 0–0 fluorescence maximum, consequently differing by a frequency of C=C stretching from the other three compounds.

All eight compounds show strong fluorescence with monoexponential decay in solution, except the low PLQY of most polar compounds in acetonitrile, where some quenching by excited-state twist may play a role. Moreover, only six of the eight compounds have a PLQY of SSF higher than 10% (Table 4), usually with multiexponential decay. Their SSF maxima relate quite well to those in DCM (Fig. 6e) for the compounds with weaker EWGs, while for compounds with stronger EWGs, the SSF spectra show a considerable blue shift with respect to fluorescence in DCM (around 90 nm for **DPA-DPS-DMV**, **-CMV** and **-CEV**), because of a limited excited-state relaxation in a rigid environment. The only exception is **DPA-DPS-DCV** with an excimer character of the solid-state emission,[34] for which only a small blue (21 nm) shift compared to DCM is observed. Otherwise, while **DPA-DPS-DMV**, **-CEV** and **-CMV** show a blue shift of the fluorescence maxima (36–53 nm, Tables S7–S9†) when going from chloroform to the solid state, **DPA-DPS-DCV** shows a red shift of 31 nm.[34] SSF maxima cover a range from 475 nm (**DPA-DPS-V**) to 733 nm (IR polymorph of **DPA-DPS-DCV**),[34] thus covering a large area of fluorescence colours in the CIE diagram (Fig. 7a). Such a range of SSF maxima, tuned only by an acceptor substituent—i.e. keeping the same donor and building block—ranks among the biggest ever reported[36,37] if expressed in wavelength scale (258 nm). Furthermore, in energy units (0.975 eV), this interval is lower than was found for simple acceptor-substituted triphenylamines (248 nm, but 1.273 eV).[38] The reason is that the conjugation extension of a bridge between the donor and acceptor from benzene to stilbene dramatically shifts the emission range from violet–red to blue–infrared (Fig. 7b), *i.e.* by about 90 nm.

While the spectral properties are mainly a function of the molecular structure, here of the EWG substituent, the photophysics is much more complicated and is driven mainly by intermolecular arrangement. An illustrative example is an almost isomorphic, π-isoelectronic **DPA-DPS-CMV** and **-CEV** pair. The SSF spectrum of the former is slightly (10 nm) red-shifted with respect to the latter, as is the case in chloroform (9 nm, Tables S8 and S9†), but its SSF PLQY is almost four times higher (Table 4) and the weighted average SSF lifetime τ is more than five times longer (Fig. 8 and Table 5). The deconvolution of SSF multiexponential decay curves (Table 5) enables the division of the set of eight compounds into three groups. The only member of the first of these groups is **DPA-DPS-DBV**, which shows an anomalous ultrashort monoexponential decay (0.42 ns), much shorter than in any solvent, and with a relatively low SSF PLQY (11%). We consider that intersystem crossing, enhanced by the heavy atom

Table 3 Comparison of the experimental and theoretical Stokes shift dependence on EWG and solvent[a]

		Toluene			Chloroform			Dichloromethane		
Compound	Experiment/theory	*A*	*F*	*S*	*A*	*F*	*S*	*A*	*F*	*S*
DPA-DPS-V	Experiment	25 840	22 520	3 320	26 040	21 320	4 720	26 040	20 700	5 340
	Theory	28 570	22 120	6 450	28 570	21 320	7 250	28 570	20 830	7 740
DPA-DPS-DMV	Experiment	24 630	18 800	5 830	24 450	15 950	8 500	24 630	15 080	9 550
	Theory	27 470	20 530	6 940	27 400	19 460	7 940	27 320	18 800	8 520
DPA-DPS-CMV	Experiment	22 370	17 240	5 130	22 220	14 860	7 360	22 370	13 720	8 650
	Theory	25 710	19 420	6 290	25 580	18 290	7 290	25 510	17 540	7 970
DPA-DPS-DCV	Experiment	21 280	16 530	4 750	20 920	14 240	6 680	21 100	13 300	7 800
	Theory	24 690	18 970	5 720	24 570	17 760	6 810	24 570	17 040	7 530

[a] Theoretical excitation energies were obtained by PCM TD DFT (CAM-B3LYP/6-311G(d,p)) calculations on the S_0 and S_1 geometries obtained on the same PCM (TD) DFT level [*A* = absorption, *F* = fluorescence and *S* = Stokes shift (all values in cm^{-1})].

Table 4 Absorption and fluorescence maxima and PLQY values in DCM and the solid state

	DCM						Solid	
Material	λ_A [nm]	ε [l mol^{-1} cm^{-1}]	λ_F [nm]	Stokes [cm^{-1}]	PLQY [%]	τ_F [ns]	λ_F [nm]	PLQY [%]
DPA-DPS-V	378	29 400	483	5751	83	1.96	475	12
DPA-DPS-DBV	386	40 000	502	5986	48	1.64	498	11
DPA-DPS-CN	393	18 000	530	6577	62	1.98	529	18
DPA-DPS-CHO[a]	408	24 800	587	7474	86	2.96	549	5
DPA-DPS-DMV	406	29 900	663	9548	46	1.45	574	20
DPA-DPS-CEV	442	27 900	716	8658	58	2.03	627	9
DPA-DPS-CMV	445	28 200	729	8754	44	1.85	637	35
DPA-DPS-DCV[b]	473	34 000	752	7844	35	1.47	733	32

[a] Polymorph G. [b] polymorph IR.

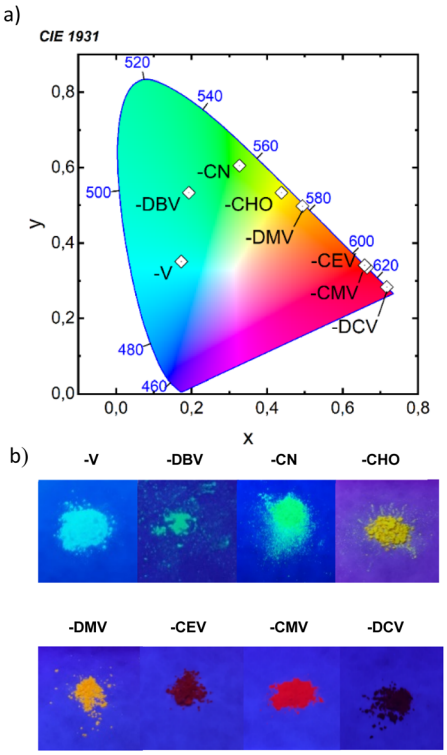

Fig. 7 Position of SSF colours in the CIE diagram (a) and photographs of powders under UV (365 nm) irradiation (b). We note that the IR SSF of DPA-DPS-DCV was outside of the detection limits of the camera.

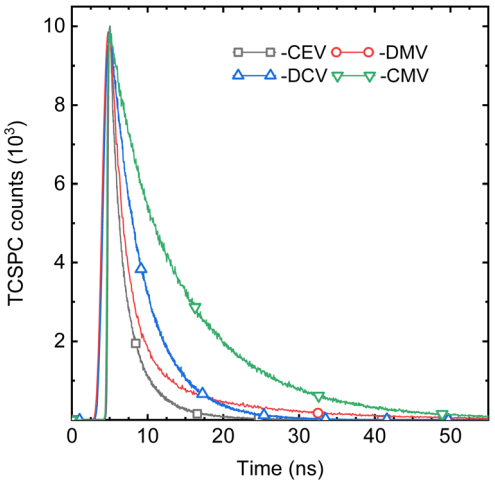

Fig. 8 Fluorescence decay curves of DPA-DPS-CEV, -DMV, -DCV and -CMV in the solid state.

effect of terminal bromines, may play a significant role,[21] but we have no experimental or theoretical evidence, so this compound was not considered. The second group contains four compounds (**DPA-DPS-V**, **-CHO**, **-CN** and **-CEV**) and is characterised by a PLQY lower than 20% (Table 4) and a significant percentage (B_1 in Table 5) of the short-lived (0.80–0.91 ns) component. The overall PLQY is the lowest (5%) for the compound (aldehyde) with the highest proportion of fast decay constant, $B_1 = 83\%$. By contrast, the highest PLQY (18%) was found for the nitrile with the lowest proportion of B_1 (46%). Thus, we consider the presence of the process, represented by this fast component, as the dominating quenching pathway. We ascribe it to energy migration, which is the most frequent reason for SSF quenching in poly- and nanocrystalline solids[20] and which manifests itself by a shortening of the lifetime with respect to monomer fluorescence, proportional to the concentration of quenching sites.[48] The dominant ($B_2 = 51\%$) portion of **DPA-DPS-CN** emission, thus, originates from monomer-like fluorescence with $\tau_2 = 2.24$ ns, which is only slightly longer than in DCM (1.98 ns, Table 4). Three compounds of the third group show a PLQY of 20% (**DPA-DPS-DMV**) and higher (**DPA-DPS-CMV** and **-DCV**), and the fast component is completely absent in their multiexponential decay (Table 5). We consider this PLQY enhancement to be a result of exciton self-trapping,[25] avoiding detrimental migration, and longer lifetimes (as compared to a monomer in solution) as a signature of aggregate emission.

TD DFT calculations on monomers and stacked dimers of the third-group compounds, with the geometries extracted from single-crystal XRD, were carried out in order to understand the character of the fluorescent traps. Directly calculated excitation energies (Table 6) were recomputed to the energy difference values (Fig. 9). All three dimers exhibit a dark lowest excited state S_1, so they can be classified as H-aggregates, even for **DPA-DPS-DMV** with a parallel arrangement of the molecules in

Table 5 Deconvolution of a multiexponential fluorescence decay in the solid state[a]

Material	τ [ns]	τ_1 [ns]	τ_2 [ns]	τ_3 [ns]	τ_4 [ns]	B_1 [%]	B_2 [%]	B_3 [%]	B_4 [%]	χ^2
DPA-DPS-V	2.20	**0.80**	2.93	5.77	—	**61**	19	20	—	1.0701
DPA-DPS-DBV	0.42	**0.42**	—	—	—	**100**	—	—	—	1.0126
DPA-DPS-CN	2.42	0.80	**2.24**	9.62	—	40	**51**	10	—	1.0896
DPA-DPS-CHO	1.84	**0.84**	—	6.75	—	**83**	—	17	—	1.1551
DPA-DPS-DMV	3.12	—	**2.25**	—	14.73	—	**93**	—	7	0.9863
DPA-DPS-CEV	1.88	**0.91**	2.25	5.05	—	**53**	35	12	—	1.0050
DPA-DPS-CMV	10.03	—	—	5.29	**11.53**	—	—	24	**76**	1.1670
DPA-DPS-DCV	4.51	—	2.76	**4.82**	—	—	15	**85**	—	1.0536

[a] Lifetimes with the highest expansion coefficients are set in bold for each compound. The weighted average fluorescence lifetime was computed according to $\tau = \Sigma B_i \tau_i$.

Table 6 TD DFT (ωB97X-D/6-311G(d,p)) excitation energies of stacked dimers in three lowest states[a]

		S_1		S_2		S_3	
Compound	Aggregate	E_{exc}	f_{osc}	E_{exc}	f_{osc}	E_{exc}	f_{osc}
DPA-DPS-DCV	Monomer	**3.275**	1.521				
	Dimer	3.093	0.000	**3.190**	2.868	3.671	0.003
DPA-DPS-CMV	Monomer	**3.401**	1.641				
	Dimer	3.261	0.000	**3.456**	2.615	3.518	0.286
DPA-DPS-DMV	Monomer	**3.564**	1.701				
	Dimer	3.507	0.000	**3.569**	3.179	3.842	0.010

[a] The excitation energies of bright monomer and dimer FR states are set in bold.

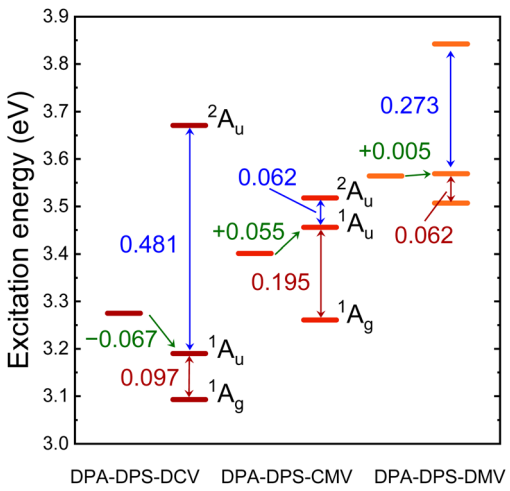

Fig. 9 Excitation energy levels of monomer S_1 state (left) and dimer S_1, S_2 and S_3 states (right) of **DPA-DPS-DCV**, **-CMV** and **-DMV**, as computed by TD DFT (ωB97X-D/6-311G(d,p)) on experimental XRD geometries. Monomer-to-dimer excitation energy shift between the lowest allowed transition is expressed in green, twice the excitonic coupling between the lower and upper Frenkel (FR) states of the dimers (S_1 and S_2) in expressed in red and the splitting between allowed FR (S_2) and charge-transfer (CT) states (S_3) is expressed in blue.

a stack.[23,24] **DPA-DPS-DCV** is the only compound which can be considered a red-shifted H-aggregate[24] according to the monomer-to-dimer energy difference. If one considers an energy difference between bright (S_2) and dark (S_1) FR states as the depth of a trap, these values (0.062 eV, 0.097 eV and 0.195 eV, Fig. 9) for **DPA-DPS-DMV**, **-DCV** and **-CMV**, respectively, qualitatively correlate to the fluorescence lifetimes with a dominating participation in SSF decay deconvolution (2.25 ns, 4.82 ns and 11.53 ns, Table 5), respectively. The energy difference between allowed FR (S_2) and CT (S_3) states, originating from TD DFT calculations, relates to the FR/CT interaction, *i.e.* the larger this difference is, the more CT character can be expected for the bright FR state.[49]

Consequently, the pronounced CT character of an emitting state can be expected for **DPA-DPS-DCV** ($\Delta E = 0.481$ eV), relating well to the red spectral shift and excimer character of SSF, while for **DPA-DPS-CMV** ($\Delta E = 0.062$ eV), the emitting state is of almost pure FR character with a slight blue shift with respect to monomer, as is usual for H-aggregates. In summary, the most intense fluorescent **DPA-DPS-CMV** derivative is, thus, quite unique, as its SSF spectrum appears to be monomer-like, but fluorescence is dramatically delayed as it originates from a deep-trap neutral H-aggregate. Thanks to the delocalisation of KS FMOs (Fig. 4 and ref. 34), the traps in **DPA-DPS-CMV** and **-DCV** crystals are localised on stacked dimers, while in **DPA-DPS-DMV**, the monomers can be considered as self-trapping sites, as both transitions to the S_1 and S_2 states are formed by symmetrical or antisymmetrical combinations of intramolecular (Fig. 4) HOMO to LUMO and HOMO−1 to LUMO+1 monoexcitations in a configurational interaction. Promoting a J-type coupling is one of the ways to enhance the PLQY of polycrystalline solids through a reduction of exciton lifetime.[20] An inclined (staircase) packing of push–pull conjugated organics may lead to abnormal photophysics, prolonging an exciton lifetime, as is the case in H-aggregates.[50] This resembles the photophysical behaviour observed in **DPA-DPS-DMV** (Fig. 2 and Table 5). We consider its moderate PLQY to be the result of an on-monomer self-trapping and small electronic coupling in terms of low values of the transfer integrals, both of which reduce the migration of an exciton, and we ascribe the slight increase of exciton lifetime to a shallow trap in a dimer approximation (Fig. 9).

Conclusions

All eight **DPA-DPS-EWG** derivatives with the same donor and building block show fluorescence both in solution and in the

solid state. The SSF maximum (colour) in powder form can be tuned by the EWG strength over a broad (from blue to infrared) range of 258 nm. Excluding intramolecular internal conversion as a decisive nonradiative deactivation channel in the solid state within the set, no significant relation between the band gap energy of the compounds and the SSF intensity was found. Exciton localisation either on a monomer (in J-like packing) or a stacked dimer (for H-aggregates) was found to be effective for improving the overall SSF PLQY through an avoidance of exciton migration to the quenching sites by a self-trapping process. The highest SSF PLQY (35%) was found for the red emission of **DPA-DPS-CMV** with the deepest trap, localised on an electronically isolated stacked dimer, causing delayed fluorescence with a lifetime more than five times longer compared to the monomer fluorescence in solution. The anomalous (with respect to other push–pull derivatives in a set) spectral shift of the SSF maximum (with respect to fluorescence in solvents) and the partial CT character of its bright state in a stacked dimer arrangement brought further evidence of an excimer character of the previously reported IR emission of **DPA-DPS-DCV**. The role of side-phenyls in the formation of beneficial structural traps in crystals is crucial, but their effect on packing is not universal, as detrimental exciton migration takes place in at least half of the derivatives under study. A relatively marginal (with respect to the molecular fluorescence in solution) change in molecular structure, such as an exchange of a methyl ester group with an ethyl ester group as an EWG substituent, causes changes in packing that are hardly predictable, switching the photophysics in the solid state from an absence to a dominance of exciton migration. We have shown here that the formation of crystal packing enabling exciton self-trapping is an efficient way to improve the SSF intensity of polycrystalline solids, but a significant amount of work on the design, syntheses and crystal engineering remains to be undertaken in order to make this method more universal.

Author contributions

The manuscript was written through contributions of all authors. All authors have given approval to the final version of the manuscript.

Conflicts of interest

There are no conflicts to declare.

Acknowledgements

The authors express their gratitude for financial support from the Czech Science Foundation, grant No. 19-22783S. Computational resources were supplied by the project "e-Infrastruktura CZ" (e-INFRA CZ LM2018140) supported by the Ministry of Education, Youth and Sports of the Czech Republic.

Notes and references

1 J. Mei, N. L. C. Leung, R. T. K. Kwok, J. W. Y. Lam and B. Z. Tang, *Chem. Rev.*, 2015, **115**, 11718–11940.
2 M. Martínez-Abadía, R. Giménez and M. B. Ros, *Adv. Mater.*, 2018, **30**, 1704161.
3 H. H. Fang, J. Yang, J. Feng, T. Yamao, S. Hotta and H. B. Sun, *Laser Photonics Rev.*, 2014, **8**, 687–715.
4 Y. Jiang, Y. Y. Liu, X. Liu, H. Lin, K. Gao, W. Y. Lai and W. Huang, *Chem. Soc. Rev.*, 2020, **49**, 5885–5944.
5 J. Zaumseil, *Adv. Funct. Mater.*, 2020, **30**, 1905269.
6 V. M. Angela, A. Anjali, D. Harshini and S. Nagarajan, *ACS Appl. Electron. Mater.*, 2021, **3**, 550–573.
7 P. Gayathri, M. Pannipara, A. G. Al-Sehemi and S. P. Anthony, *New J. Chem.*, 2020, **44**, 8680–8696.
8 J. Zhang, B. He, Y. Hu, P. Alam, H. Zhang, J. W. Y. Lam and B. Z. Tang, *Adv. Mater.*, 2021, **33**, 2008071.
9 Q. Wei, N. Fei, A. Islam, T. Lei, L. Hong, R. Peng, X. Fan, L. Chen, P. Gao and Z. Ge, *Adv. Opt. Mater.*, 2018, **6**, 1800512.
10 G. Hong, X. Gan, C. Leonhardt, Z. Zhang, J. Seibert, J. M. Busch and S. Bräse, *Adv. Mater.*, 2021, **33**, 2005630.
11 Ch. Adachi and A. S. D. Sandanayaka, *CCS Chem.*, 2020, **2**, 1203–1216.
12 H. Nakanotani, Y. Tsuchiya and C. Adachi, *Chem. Lett.*, 2021, **50**, 938–948.
13 Y. Xu, P. Xu, D. Hu and Y. Ma, *Chem. Soc. Rev.*, 2021, **50**, 1030–1069.
14 Z. Zheng, T. Zhang, H. Liu, Y. Chen, R. T. K. Kwok, C. Ma, P. Zhang, H. H. Y. Sung, I. D. Williams, J. W. Y. Lam, K. S. Wong and B. Z. Tang, *ACS Nano*, 2018, **12**, 8145–8159.
15 J. Qi, X. Duan, Y. Cai, S. Jia, C. Chen, Z. Zhao, Y. Li, H. Q. Peng, R. T. K. Kwok, J. W. Y. Lam, D. Ding and B. Z. Tang, *Chem. Sci.*, 2020, **11**, 8438–8477.
16 W. L. Algar, M. Massey, K. Rees, R. Higgins, K. D. Krause, G. H. Darwish, W. J. Peveler, Z. Xiao, H. Y. Tsai, R. Gupta, K. Lix, M. V. Tran and H. Kim, *Chem. Rev.*, 2021, **121**, 9243–9358.
17 J. Wang, L. Zhang and Z. Li, *Adv. Healthcare Mater.*, 2021, **10**, 2101169.
18 Y. Wang, B. Xia, Q. Huang, T. Luo, Y. Zhang, P. Timashev, W. Guo, F. Li and X. J. Liang, *Adv. Healthcare Mater.*, 2021, **10**, 2100945.
19 K. Li, T. B. Ren, S. Huan, L. Yuan and X. B. Zhang, *J. Am. Chem. Soc.*, 2021, **143**, 21143–21160.
20 J. Gierschner, J. Shi, B. Milián-Medina, D. Roca-Sanjuán, S. Varghese and S. Y. Park, *Adv. Opt. Mater.*, 2021, **9**, 2002251.
21 D. Sasikumar, A. T. John, J. Sunny and M. Hariharan, *Chem. Soc. Rev.*, 2020, **49**, 6122–6140.
22 J. Mei, Y. Hong, J. W. Y. Lam, A. Qin, Y. Tang and B. Z. Tang, *Adv. Mater.*, 2014, **26**, 5429–5479.
23 N. J. Hestand and F. C. Spano, *Chem. Rev.*, 2018, **118**, 7069–7163.
24 C. Zheng, C. Zhong, C. J. Collison and F. C. Spano, *J. Phys. Chem. C*, 2019, **123**, 3203–3215.
25 O. P. Dimitriev, *Chem. Rev.*, 2022, **122**(9), 8487–8593.
26 A. Zampetti, A. Minotto and F. Cacialli, *Adv. Funct. Mater.*, 2019, **29**, 1807623.
27 L. M. Ibele, P. A. Sánchez-Murcia, J. J. Nogueira and L. González, *J. Phys. Chem. Lett.*, 2020, **11**, 7483–7488.
28 Y. Shen, Z. Zhang, H. Liu, Y. Yan, S. Zhang, B. Yang and Y. Ma, *J. Phys. Chem. C*, 2019, **123**, 13047–13056.

29 H. Liu, L. Yao, B. Li, X. Chen, Y. Gao, S. Zhang, W. Li, P. Lu, B. Yang and Y. Ma, *Chem. Commun.*, 2016, **52**, 7356–7359.
30 Y. Shen, H. Liu, S. Zhang, Y. Gao, B. Li, Y. Yan, Y. Hu, L. Zhao and B. Yang, *J. Mater. Chem. C*, 2017, **5**, 10061–10067.
31 Q. Luo, L. Li, H. Ma, C. Lv, X. Jiang, X. Gu, Z. An, B. Zou, C. Zhang and Y. Zhang, *Chem. Sci.*, 2020, **11**, 6020–6025.
32 Z. Sun, Q. Zang, Q. Luo, C. Lv, F. Cao, Q. Song, R. Zhao, Y. Zhang and W. Y. Wong, *Chem. Commun.*, 2019, **55**, 4735–4738.
33 C. Lv, W. Liu, Q. Luo, H. Yi, H. Yu, Z. Yang, B. Zou and Y. Zhang, *Chem. Sci.*, 2020, **11**, 4007–4015.
34 K. Pauk, S. Luňák Jr, A. Růžička, A. Marková, A. Mausová, M. Kratochvíl, K. Melánová, M. Weiter, A. Imramovský and M. Vala, *Chem.–Eur. J.*, 2021, **27**, 4341–4348.
35 M. Shimizu and T. Hiyama, *Chem.–Asian J.*, 2010, **5**, 1516–1531.
36 M. K. Bera, P. Pal and S. Malik, *J. Mater. Chem. C*, 2020, **8**, 788–802.
37 M. Shimizu, *Chem. Rec.*, 2021, **21**, 1489–1505.
38 E. Ishow, A. Brosseau, G. Clavier, K. Nakatani, P. Tauc, C. Fiorini-Debuisschert, S. Neveu, O. Sandre and A. Léaustic, *Chem. Mater.*, 2008, **20**, 6597–6599.
39 S. Kundu, B. Sk, P. Pallavi, A. Giri and A. Patra, *Chem.–Eur. J.*, 2020, **26**, 5557–5582.
40 M. J. Frisch, W. G. Trucks, H. B. Schlegel, G. E. Scuseria, M. A. Robb, J. R. Cheeseman, G. Scalmani, V. Barone, B. G. Mennucci, A. Petersson, H. Nakatsuji, M. Caricato, X. Li, H. P. Hratchian, A. F. Izmaylov, J. Bloino, G. Zheng, J. L. Sonnenberg, M. Hada, M. Ehara, K. Toyota, R. Fukuda, J. Hasegawa, M. Ishida, T. Nakajima, Y. Honda, O. Kitao, H. Nakai, T. Vreven, J. A. Montgomery Jr, J. E. Peralta, F. Ogliaro, M. Bearpark, J. J. Heyd, E. Brothers, K. N. Kudin, V. N. Staroverov, R. Kobayashi, J. Normand, K. Raghavachari, A. Rendell, J. C. Burant, S. S. Iyengar, J. Tomasi, M. Cossi, N. Rega, J. M. Millam, M. Klene, J. E. Knox, J. B. Cross, V. Bakken, C. Adamo, J. Jaramillo, R. Gomperts, R. E. Stratmann, O. Yazyev, A. J. Austin, R. Cammi, C. Pomelli, J. W. Ochterski, R. L. Martin, K. Morokuma, V. G. Zakrzewski, G. A. Voth, P. Salvador, J. J. Dannenberg, S. Dapprich, A. D. Daniels, Ö. Farkas, J. B. Foresman, J. V. Ortiz, J. Cioslowski, D. J. Fox and C. T. Wallingford, *Gaussian 09, Revision D.01*, Gaussian, Inc., 2009.
41 Y. D. Lin, Y. S. Pen, W. Su, K. L. Liau, Y. S. Wen, C. H. Tu, C. H. Sun and T. J. Chow, *Chem.–Asian J.*, 2012, **7**, 2864–2871.
42 C. Coluccini, A. K. Sharma, M. Caricato, A. Sironi, E. Cariati, S. Righetto, E. Tordin, C. Botta, A. Forni and D. Pasini, *Phys. Chem. Chem. Phys.*, 2013, **15**, 1666–1674.
43 C. R. Martinez and B. L. Iverson, *Chem. Sci.*, 2012, **3**, 2191–2201.
44 N. J. Hestand and F. C. Spano, *Acc. Chem. Res.*, 2017, **50**, 341–350.
45 A. A. Isse and A. Gennaro, *J. Phys. Chem. B*, 2010, **114**, 7894–7899.
46 B. Kumari, A. Singh, P. Jana, M. Radhakrishna and S. Kanvah, *New J. Chem.*, 2019, **43**, 11701–11709.
47 F. C. Spano, *Acc. Chem. Res.*, 2010, **43**, 429–439.
48 O. V. Mikhnenko, P. W. M. Blom and T. Q. Nguyen, *Energy Environ. Sci.*, 2015, **8**, 1867–1888.
49 S. Canola, G. Bagnara, Y. Dai, G. Ricci, A. Calzolari and F. Negri, *J. Chem. Phys.*, 2021, **154**, 124101.
50 J. Xue, Q. Liang, R. Wang, J. Hou, W. Li, Q. Peng, Z. Shuai and J. Qiao, *Adv. Mater.*, 2019, **31**, 1808242.
51 J. D. Chai and M. Head-Gordon, *Phys. Chem. Chem. Phys.*, 2008, **10**, 6615–6620.
52 T. Yanai, D. P. Tew and N. C. Handy, *Chem. Phys. Lett.*, 2004, **393**, 51–57.